

Observational Relationship between Spectral Properties of Gamma-ray and X-ray Emissions from Pulsars

Ashwin Aravindaraj,¹★ and Hsiang-Kuang Chang,^{1,2,3,4}†

¹*Institute of Astronomy, National Tsing Hua University, Hsinchu 300044, Taiwan*

²*Department of Physics, National Tsing Hua University, Hsinchu 300044, Taiwan*

³*Institute of Space Engineering, National Tsing Hua University, Hsinchu 300044, Taiwan*

⁴*Center for Theory-Computation-Data Science Research (CTCD), National Tsing Hua University, Hsinchu 300044, Taiwan*

arXiv:2601.13557v1 [astro-ph.HE] 20 Jan 2026

Accepted XXX. Received YYY; in original form ZZZ

ABSTRACT

Correlations between gamma-ray and X-ray spectral properties of pulsars are investigated in order to provide observational hints on physics involved in pulsars' high-energy emissions. Using a sample of 43 pulsars detected in both X-ray and gamma-ray bands, we find that pulsars' gamma-ray luminosity, L_γ , clearly correlates with the luminosity of non-thermal X-ray emission, L_p , and anti-correlates with non-thermal X-ray photon index. Other gamma-ray spectral parameters show weaker or negligible correlations. The found relation that $L_\gamma \propto L_p^{0.49 \pm 0.05}$ implies a certain connection between radiation mechanisms and energy distributions of radiating particles for these high-energy emissions. Pulsars with and without detected thermal emissions seem to show different dependencies in those correlations, suggesting the possible existence of two different kinds of pulsars. The ones without detected thermal emissions may represent a population of pulsars with low surface temperature. The origin and energetics of high-energy emitting electron-positron pairs for this group of pulsars probably do not depend on their surface thermal emissions, while that of the other group do. The low surface temperatures might be evidence for the working of some exotic processes of neutron-star cooling. Similar to L_p , some tempting relationships are found among each gamma-ray spectral parameter, surface temperature and thermally radiating area radius. It again strengthens the connection between gamma-ray and X-ray emissions from pulsars.

Key words: radiation mechanisms: non-thermal – radiation mechanisms: thermal – pulsars: general – gamma-rays: stars – X-rays: stars

1 INTRODUCTION

Pulsars are observed in electromagnetic radiation from radio to gamma rays. About four thousand are observed in the radio band (see the ATNF catalog (Manchester et al. (2005))) and 294 in gamma-rays (see the Third Fermi LAT Catalog of Gamma-ray Pulsars (Smith et al. 2023); hereafter 3PC). Pulsars' radio emissions are considered to be from a certain kind of coherent mechanism, but emissions at higher energies are not. Although there is no demand on devising a coherent mechanism for these high-energy emissions, the origin and mechanisms of pulsar high-energy emissions are still in debate.

Models for high energy emissions from pulsars have evolved from the earlier polar-gap (Daugherty & Harding (1982)), slot-gap (Arons (1983)), outer-gap (Cheng et al. 1986), and striped-wind (Coroniti (1990); Michel (1994); Kirk et al. (2002)) models to more recent, more involved ones, which include, for example, the striped-wind model with particle-in-cell simulations (Pétri (2024); Cerutti et al. (2025)), the extended-slot-gap and equatorial-current-sheet model (Harding et al. (2021); Barnard et al. (2022)), the synchro-curvature

model (Torres et al. (2019); Íñiguez-Pascual et al. (2022)) and the non-stationary outer-gap model (Takata & Cheng (2017)).

A comprehensive picture to understand all the properties of high-energy emissions across different energy bands, from optical to gamma rays, has not yet appeared in current models. In observational aspect, population studies on cross-band correlations are very few. Most are on the correlation between spectral properties of a certain band and timing parameters (e.g. Possenti et al. (2002); Li et al. (2008); Chang et al. (2023)) or on spectral properties in a certain band for a certain group of pulsars, such as non-thermal X-ray emissions from gamma-ray pulsars (Coti Zelati et al. 2020). We therefore conduct an effort to investigate possible correlations between spectral properties of GeV gamma-ray emission and X rays from pulsars. These correlations may inspire and constrain modelling works.

Fermi LAT has significantly increased the number of gamma-ray pulsars to 294 (3PC). Gamma-ray spectra of these pulsars are described in great details in 3PC with a particular cut-off power-law model (Eq.(15) in Smith et al. (2023)). In this paper, we report the results of examining correlations between spectral properties of gamma-ray and X-ray emissions from pulsars.

Besides those consistent with earlier literature, we found that the gamma-ray luminosity clearly correlates with the luminosity of non-

★ E-mail: ashwinaravindaraj@gmail.com

† E-mail: hkchang@mx.nthu.edu.tw

thermal X-ray emission and anti-correlates with its photon index. Pulsars with and without detected thermal emissions seem to show different dependencies in those relations, suggesting possible existence of two different kinds of pulsars.

In Section 2 we explain the data selection criteria. Correlation analysis results are presented in Section 3. The dependence of the gamma-ray luminosity and other spectral parameters on timing parameters is shown in Section 3.1 as a check with earlier literature.

Then the relationships between gamma-ray and non-thermal X-ray emissions are reported in Section 3.2. That between gamma-ray and thermal X-ray emissions are presented in Section 3.3. Correlations among gamma-ray spectral parameters are shown in Section 3.4. Discussions on these results are in Section 4.

2 SAMPLE SELECTION

To collect samples for this study, we cross-matched the list of pulsars with X-ray emissions reported in Chang et al. (2023) with 3PC and found 43 pulsars with both GeV gamma-ray and X-ray emissions. We note that about 200 more candidates of pulsars with X-ray emissions have been reported based on position coincidence and flux ratios in different wave bands (Mayer & Becker (2024); Xu et al. (2025)). Future confirmation of these candidates will further increase the sample size. Among these 43 pulsars, PSR J2021+4026 is observed to switch between two gamma-ray emission states, with flux in $0.1 - 100$ GeV being $(6.86 \pm 0.13) \times 10^{-10}$ erg cm $^{-2}$ s $^{-1}$ (Al-lafont et al. (2013)) and $(8.33 \pm 0.08) \times 10^{-10}$ erg cm $^{-2}$ s $^{-1}$ (Zhao et al. (2017)), respectively. Its X-ray flux (0.2 keV – 12 keV) is found to be $3.5_{-0.7}^{+1.3} \times 10^{-14}$ erg cm $^{-2}$ s $^{-1}$ (Lin et al. (2013)) and $4.7_{-1.0}^{+1.4} \times 10^{-14}$ erg cm $^{-2}$ s $^{-1}$ (Wang et al. (2018)) correspondingly and there is a 6% change in the time derivative of its period between the two states (see Figure 1 in Wang et al. (2024)). This pulsar in different states is treated as two pulsars in this study. Hereafter we therefore refer to the number of pulsars in our sample as 44.

Among the 44 pulsars in this study, the X-ray spectra of 22 pulsars are well fitted by a power law. Another 18 can be well described by a two-component model of a power law plus a blackbody. For the other four, that is, PSR J0633+1746, PSR J0659+1414, PSR J1057-5226, and PSR J1740+1000, a three-component model consisting of a power law plus two blackbodies is required. To have a uniform comparison base, a flux-weighted average of the temperature and the emitting-region radius of the two blackbody components, as reported in Chang et al. (2023), is adopted to describe their thermal emission.

To calculate luminosity from flux, we consider the luminosity ($L = 4\pi d^2 f_\Omega F$) with a beaming fraction of $f_\Omega = 1$ (Watters et al. 2009) and use distance estimates from various independent measurements, along with their associated uncertainties listed in the ATNF catalog (Manchester et al. 2005), whenever available. If there are no independent measurements, we adopt the dispersion-measure-based distance estimate (also provided in the ATNF catalog) and assign, following Li et al. (2008) and Chang et al. (2023), a 40% uncertainty to the distance. Due to the large uncertainty in distances, we use the Monte Carlo error propagation method to derive luminosity errors. The X-ray luminosity of the power-law component, L_p , reported in this study is for the energy range of 0.5 – 8 keV, and the gamma-ray one, L_γ , is from 0.1 to 100 GeV. All the gamma-ray fluxes are taken from 3PC.

The timing variables and distances taken from the ATNF catalog are shown in Table 1. The gamma-ray spectral parameters listed in Table 2 are taken directly from 3PC, where Γ_{100} denotes the photon index, E_p the peak energy, and d_p the curvature of the gamma-ray

spectrum around the peak energy; readers are referred to 3PC for details. The X-ray spectral properties of these 44 pulsars are also listed in Table 2.

3 CORRELATION ANALYSIS

In this section, we report results of studying the correlation between GeV gamma-ray and keV X-ray spectral properties of the 44 pulsars in the hope to shed some light on our understanding of pulsar emission mechanisms. The Spearmann rank-order coefficient, r_s , and its corresponding p-value are employed to indicate the significance of a possible correlation between two physical quantities. The best linear fit for these parameters is calculated with the orthogonal distance regression (ODR) method when both variables have quoted errors. Otherwise, the weighted least squares method is used for the fitting.

3.1 Correlation between gamma-ray spectral properties and timing parameters

We examine the correlation between gamma-ray spectral properties and the timing parameters for the 44 pulsars in our sample to verify consistency with previous studies. Specifically, we examine their relations with period (P), period derivative (\dot{P}), spin-down power (\dot{E}), characteristic age (τ), surface magnetic field (B_s), and magnetic field at the light cylinder (B_{lc}). The definitions of these parameters are in the caption of Table 1.

One can see that the gamma-ray luminosity is clearly correlated with timing variables P , \dot{P} , τ and \dot{E} (Fig. 1). The best fit for these relations are

$$L_\gamma \propto P^{-2.81 \pm 0.49} \quad (\chi^2_\nu = 57.6) \quad (1)$$

$$L_\gamma \propto \dot{P}^{1.33 \pm 0.24} \quad (\chi^2_\nu = 59.6) \quad (2)$$

$$L_\gamma \propto \dot{E}^{0.82 \pm 0.1} \quad (\chi^2_\nu = 36.6) \quad (3)$$

$$L_\gamma \propto \tau^{-1.29 \pm 0.16} \quad (\chi^2_\nu = 40.4) \quad (4)$$

The relation between the gamma-ray luminosity and the spindown power (the middle-right panel in Fig. 1 and Eq.(3)) is consistent with those shown in Figure 9 of Abdo et al. (2013) and in Figure 23 of Smith et al. (2023).

We note that all the above reported χ^2_ν and those in the following are only suggestive for various reasons, such as unknown beaming factors, viewing geometry and distance uncertainties. There is usually a large scatter in the correlation among spectral and timing parameters, as discussed in Possenti et al. (2002), Li et al. (2008) and Chang et al. (2023). Furthermore, in those earlier works, the distance uncertainty is all set to be 40%. Typical χ^2_ν obtained for those best linear fitting is around 3 or 4. In this work, we adopt the uncertainties associated with the reported distance estimates, most of which are smaller than 40%. The best-fit χ^2_ν is therefore much larger than those in earlier literature.

We also found that the gamma-ray luminosity is strongly correlated with B_{lc} with a Spearmann coefficient of 0.71 but it does not seem to be correlated with the surface magnetic field (B_s) as shown in Fig. 1. The relationship of the gamma-ray luminosity with B_{lc} follows as

$$L_\gamma \propto B_{lc}^{1.11 \pm 0.14} \quad (\chi^2_\nu = 40.7) \quad (5)$$

Table 1. Timing variables of the 44 pulsars. P is the pulsar period and \dot{P} is its first time derivative. Other timing variables, the spin-down power \dot{E} , characteristic age τ , surface dipole magnetic field strength B_s , and magnetic field strength at the light cylinder B_{lc} , are all functions of P and \dot{P} . With the conventional values of the moment of inertia as 10^{45} g cm 2 and neutron star radius as 10 km for the pulsar, these variables are (all in gaussian units) $\dot{E} = 3.9 \times 10^{46} P^{-3} \dot{P}$, $\tau = 0.5 P \dot{P}^{-1}$, $B_s = 3.2 \times 10^{19} (P \dot{P})^{0.5}$, and $B_{lc} = 2.9 \times 10^8 P^{-2.5} \dot{P}^{0.5}$.

Pulsars	Distances (kpc)	P (s)	\dot{P} (s/s)	\dot{E} (erg/sec)	τ (years)	B_s (gauss)	B_{lc} (gauss)
J0007+7303	1.4 ± 0.3	0.3159	3.56×10^{-13}	4.45×10^{35}	1.39×10^4	1.08×10^{13}	3.08×10^3
J0205+6449	3.2 ± 0.2	0.0657	1.92×10^{-13}	2.67×10^{37}	5.37×10^3	3.61×10^{12}	1.15×10^5
J0357+3205	0.6 ± 0.3	0.44	1.31×10^{-14}	5.9×10^{33}	5.4×10^5	2.43×10^{12}	2.53×10^2
J0534+2200	$2^{+0.4}_{-0.3}$	0.03	4.2×10^{-13}	4.35×10^{38}	1.26×10^3	3.79×10^{12}	9.01×10^5
J0540-6919	49.7 ± 1.1	0.05	4.79×10^{-13}	1.46×10^{38}	1.67×10^3	4.98×10^{12}	3.48×10^5
J0633+0632	1.35 ± 0.65	0.297	7.96×10^{-14}	1.19×10^{35}	5.92×10^4	4.92×10^{12}	1.7×10^3
J0633+1746	0.2 ± 0.1	0.237	1.1×10^{-14}	3.25×10^{34}	3.42×10^5	1.63×10^{12}	1.11×10^3
J0659+1414	0.29 ± 0.03	0.385	5.5×10^{-14}	3.8×10^{34}	1.11×10^5	4.65×10^{12}	7.4×10^2
J0835-4510	0.28 ± 0.02	0.089	1.22×10^{-13}	6.76×10^{36}	1.13×10^4	3.38×10^{12}	4.24×10^4
J0922+0638	$1.1^{+0.2}_{-0.1}$	0.43	1.37×10^{-14}	6.77×10^{33}	4.97×10^5	2.46×10^{12}	2.79×10^2
J1016-5857	3.16 ± 1.26	0.107	8.04×10^{-14}	2.56×10^{36}	2.1×10^4	2.98×10^{12}	2.18×10^4
J1023-5746	$4.02^{+0.08}_{-0.12}$	0.11	3.8×10^{-13}	1.08×10^{37}	4.6×10^3	6.62×10^{12}	4.31×10^4
J1048-5832	$2.9^{+1.2}_{-0.7}$	0.124	9.55×10^{-14}	1.99×10^{36}	2.04×10^4	3.49×10^{12}	1.67×10^4
J1057-5226	0.09 ± 0.04	0.197	5.8×10^{-15}	3.01×10^{34}	5.35×10^5	1.09×10^{12}	1.28×10^3
J1112-6103	4.46 ± 1.79	0.065	3.15×10^{-14}	4.54×10^{36}	3.27×10^4	1.45×10^{12}	4.78×10^4
J1124-5916	$4.8^{+1.2}_{-0.7}$	0.135	7.52×10^{-13}	1.19×10^{37}	2.85×10^3	1.02×10^{13}	3.72×10^4
J1357-6429	3.1 ± 1.24	0.166	3.54×10^{-13}	3.05×10^{36}	7.31×10^3	7.83×10^{12}	1.53×10^4
J1418-6058	1.6 ± 0.7	0.11	1.71×10^{-13}	4.99×10^{36}	1.03×10^4	4.38×10^{12}	2.95×10^4
J1420-6048	5.63 ± 2.25	0.0682	8.24×10^{-14}	1.03×10^{37}	1.3×10^4	2.41×10^{12}	6.85×10^4
J1459-6053	$2.27^{+1.38}_{-0.632}$	0.103	2.53×10^{-14}	9.08×10^{35}	6.47×10^4	1.63×10^{12}	1.35×10^4
J1509-5850	3.37 ± 1.35	0.089	9.2×10^{-15}	5.16×10^{35}	1.54×10^5	9.14×10^{11}	1.18×10^4
J1709-4429	$2.6^{+0.5}_{-0.6}$	0.102	9.48×10^{-14}	3.48×10^{36}	1.75×10^4	3.12×10^{12}	2.65×10^4
J1718-3825	3.49 ± 1.4	0.075	1.32×10^{-14}	1.25×10^{36}	8.95×10^4	1.01×10^{12}	2.18×10^4
J1732-3131	0.64 ± 0.26	0.196	2.8×10^{-14}	1.45×10^{35}	1.11×10^5	2.38×10^{12}	2.84×10^3
J1740+1000	1.23 ± 0.49	0.154	2.13×10^{-14}	2.30×10^{35}	1.14×10^5	1.84×10^{12}	4.54×10^3
J1741-2054	$0.3^{+0.7}_{-0.1}$	0.413	1.7×10^{-14}	9.48×10^{33}	3.86×10^5	2.68×10^{12}	3.43×10^2
J1747-2958	2.52 ± 1	0.098	6.13×10^{-14}	2.51×10^{36}	2.55×10^4	2.49×10^{12}	2.34×10^4
J1801-2451	3.8 ± 1.52	0.125	8.95×10^{-14}	1.81×10^{36}	1.55×10^4	4.04×10^{12}	1.57×10^4
J1809-2332	1.7 ± 1	0.147	3.44×10^{-14}	4.29×10^{35}	6.76×10^4	2.27×10^{12}	6.51×10^3
J1813-1246	2.64 ± 0.14	0.048	1.76×10^{-14}	6.24×10^{36}	4.34×10^4	9.3×10^{11}	7.58×10^4
J1826-1256	3.5 ± 0.1	0.11	1.21×10^{-13}	3.56×10^{36}	1.44×10^4	3.7×10^{12}	2.5×10^4
J1833-1034	4.1 ± 0.3	0.062	2.02×10^{-13}	3.36×10^{37}	4.85×10^3	3.58×10^{12}	1.37×10^5
J1836+5925	0.5 ± 0.3	0.173	1.5×10^{-15}	1.14×10^{34}	1.83×10^6	5.16×10^{11}	8.98×10^2
J1838-0537	$4.02^{+2.47}_{-1.13}$	0.146	4.51×10^{-13}	5.75×10^{36}	4.89×10^3	8.39×10^{12}	2.4×10^4
J1907+0602	2.6 ± 1.04	0.106	8.65×10^{-14}	2.81×10^{36}	1.95×10^4	3.08×10^{12}	2.30×10^4
J1952+3252	3 ± 2	0.039	5.8×10^{-15}	3.72×10^{36}	1.07×10^5	4.86×10^{11}	7.12×10^4
J1957+5033	0.55 ± 0.45	0.374	7.08×10^{-15}	5.31×10^{33}	8.39×10^5	1.65×10^{12}	2.84×10^2
J2021+3651	$1.8^{+1.7}_{-1.4}$	0.104	9.48×10^{-14}	3.35×10^{36}	1.72×10^4	3.19×10^{12}	2.58×10^4
J2021 + 4026 _{LGF}	2.15 ± 0.45	0.2653	5.77×10^{-14}	1.22×10^{35}	7.28×10^4	3.97×10^{12}	1.93×10^3
J2021 + 4026 _{HGF}	2.15 ± 0.45	0.2653	5.45×10^{-14}	1.14×10^{35}	7.71×10^4	3.85×10^{12}	1.87×10^3
J2022+3842	10^{+4}_{-2}	0.048	8.62×10^{-14}	2.97×10^{37}	8.94×10^3	2.07×10^{12}	1.64×10^5
J2043+2740	1.48 ± 0.592	0.096	1.2×10^{-15}	5.5×10^{34}	1.2×10^6	3.54×10^{11}	3.51×10^3
J2055+2539	0.62 ± 0.15	0.32	4.1×10^{-15}	4.96×10^{33}	1.24×10^6	1.16×10^{12}	3.22×10^2
J2229+6114	3 ± 1.2	0.052	7.53×10^{-14}	2.16×10^{37}	1.05×10^4	2.03×10^{12}	1.31×10^5

Since the above timing parameters are all functions of P and \dot{P} , a generic description for the gamma-ray luminosity as a function of P and \dot{P} might also be helpful. The best fit of such a function for our sample pulsars is

$$L_\gamma \propto P^{-2.17 \pm 0.41} \dot{P}^{1.01 \pm 0.20} \quad (6)$$

This best fit does not improve the fitting in terms of χ^2_ν . However, it shows that \dot{E} , which is proportional to $P^{-3} \dot{P}$, is the most relevant quantity to the gamma-ray luminosity among all the timing parameters.

The relationship between other gamma-ray spectral parameters and the timing properties of pulsars are shown in Fig. A1-A3. Since their correlations are all weak or negligible, they are put in the

Appendix to allow a better reading fluence in the main text. **Overall**, among the gamma-ray spectral properties of the 44 pulsars with X-ray emissions, only L_γ shows clear correlations with P , \dot{P} , \dot{E} , τ and B_{lc} .

3.2 Correlation of gamma-ray spectral properties with non-thermal X-ray emissions

We check the correlation between gamma-ray spectral parameters (L_γ , Γ_{100} , d_p , E_p) and the non-thermal X-ray spectral parameters (L_p , Γ_p). They are shown in Fig. 2 & 3.

For the relation between the gamma-ray luminosity and non-thermal X-ray emission, represented by the power-law component

Table 2. Spectral properties of the 44 pulsars. Columns 2-5 list gamma-ray emission properties. Γ_{100} denotes the photon index, E_p the peak energy, and d_p the curvature of the gamma-ray spectrum around the peak energy. Columns 6-10 are of X-rays. Γ_p is the power-law photon index of the X-ray spectrum. kT is the surface temperature and R is the emission radius from the X-ray spectral fitting. Those pulsars without kT and R information are designated as Group 1 pulsars and the others are Group 2 ones. X-ray spectral information is from the following references listed in the last column: (1) Chang et al. (2023) (2) Marelli et al. (2013) (3) Li et al. (2008) (4) Ge et al. (2019) (5) Danilenko et al. (2015) (6) Posselt et al. (2017) (7) De Luca et al. (2005) (8) Pavlov et al. (2001) (9) Rigoselli & Mereghetti (2018) (10) Klingler et al. (2022) (11) Kargaltsev et al. (2007) (12) Posselt et al. (2015) (13) Chang et al. (2012) (14) Kim & An (2020) (15) Pancrazi et al. (2012) (16) Klingler et al. (2016) (17) Romani et al. (2005) (18) Rigoselli et al. (2022) (19) Karpova et al. (2014) (20) Klingler et al. (2018) (21) Kaspi et al. (2001) (22) Karpova et al. (2019) (23) Lin et al. (2014) (24) Coti Zelati et al. (2020) (25) Li et al. (2005) (26) Zyuzin et al. (2021) (27) Van Etten et al. (2008) (28) Lin et al. (2013) (29) Allafort et al. (2013) (30) Wang et al. (2018) (31) Zhao et al. (2017) (32) Becker et al. (2004) (33) Marelli et al. (2016)

Pulsars	L_γ (erg/sec)	Γ_{100}	E_p (GeV)	d_p	L_p (erg/sec)	Γ_p	kT (eV)	R (km)	References
J0007+7303	$1.01^{+0.48}_{-0.39} \times 10^{35}$	1.2 ± 0.04	2.44 ± 0.03	0.36 ± 0.01	$8.81^{+4.3}_{-3.41} \times 10^{30}$	$1.71^{+0.3}_{-0.28}$	–	–	1
J0205+6449	$7.85^{+1.04}_{-0.97} \times 10^{34}$	1.6 ± 0.22	0.26 ± 0.1	0.45 ± 0.08	$1.06^{+0.14}_{-0.13} \times 10^{33}$	$1.47^{+0.03}_{-0.03}$	167^{+31}_{-19}	$1.3^{+2.02}_{-1.06}$	1
J0357+3205	$2.58^{+3.22}_{-1.94} \times 10^{33}$	0.73 ± 0.23	0.87 ± 0.03	0.95 ± 0.05	$1.75^{+2.19}_{-1.3} \times 10^{30}$	$2.28^{+0.17}_{-0.16}$	94^{+12}_{-9}	$0.54^{+0.81}_{-0.49}$	2
J0534+2200	$7.17^{+2.7}_{-2.3} \times 10^{35}$	2 ± 0.03	0.04 ± 0.03	0.23 ± 0.01	$1.32^{+0.61}_{-0.46} \times 10^{36}$	$1.63^{+0.09}_{-0.09}$	–	–	3
J0540-6919	$7.94^{+0.57}_{-0.56} \times 10^{36}$	–	0.02 ± 0.08	0.26 ± 0.05	$3^{+0.2}_{-0.19} \times 10^{36}$	$0.78^{+0.09}_{-0.09}$	–	–	3,4
J0633+0632	$2.10^{+2.47}_{-1.51} \times 10^{34}$	1.1 ± 0.17	1.43 ± 0.06	0.6 ± 0.03	$1.29^{+2.35}_{-0.92} \times 10^{31}$	$1.6^{+0.6}_{-0.6}$	105^{+23}_{-18}	$3.24^{+11.68}_{-2.86}$	5
J0633+1746	$2.01^{+2.48}_{-1.49} \times 10^{34}$	1.1 ± 0.01	1.63 ± 0.01	0.66 ± 0.0001	$1.64^{+2.04}_{-1.22} \times 10^{30}$	$1.47^{+0.06}_{-0.07}$	72^{+4}_{-4}	$2.24^{+2.19}_{-2.07}$	6
J0659+1414	$2.72^{+0.6}_{-0.54} \times 10^{32}$	1.5 ± 0.27	0.16 ± 0.03	0.86 ± 0.09	$1.51^{+0.64}_{-0.54} \times 10^{30}$	$2.30^{+0.68}_{-0.57}$	66^{+3}_{-6}	$0.41^{+0.36}_{-0.25}$	7
J0835-4510	$8.72^{+1.28}_{-1.19} \times 10^{34}$	1.4 ± 0.01	1.27 ± 0.01	0.52 ± 0.0001	$5.27^{+1.13}_{-1} \times 10^{32}$	$2.7^{+0.4}_{-0.4}$	128^{+3}_{-3}	$2.35^{+1.57}_{-1.44}$	8
J0922+0638	$3.18^{+1.15}_{-0.92} \times 10^{32}$	–	–	0.12 ± 0.16	$1.53^{+0.95}_{-0.75} \times 10^{30}$	$2.20^{+0.6}_{-0.6}$	110^{+20}_{-30}	$0.21^{+0.34}_{-0.16}$	9
J1016-5857	$8.36^{+8.07}_{-5.3} \times 10^{34}$	1.5 ± 0.58	0.89 ± 0.3	0.63 ± 0.1	$7.2^{+6.84}_{-4.61} \times 10^{32}$	$1.08^{+0.08}_{-0.08}$	–	–	10
J1023-5746	$2.9^{+3.16}_{-2} \times 10^{35}$	–	0.62 ± 0.13	0.67 ± 0.06	$8.46^{+9.23}_{-5.83} \times 10^{33}$	$0.84^{+0.42}_{-0.42}$	–	–	1
J1048-5832	$1.91^{+1.45}_{-1.06} \times 10^{35}$	1.2 ± 0.15	0.97 ± 0.07	0.41 ± 0.02	$2.42^{+1.91}_{-1.31} \times 10^{31}$	$1.5^{+0.3}_{-0.3}$	–	–	11
J1057-5226	$3.1^{+2.97}_{-1.97} \times 10^{32}$	1 ± 0.06	1.21 ± 0.01	0.88 ± 0.02	$8.4^{+1.04}_{-0.54} \times 10^{28}$	$1.9^{+0.2}_{-0.2}$	85^{+6}_{-6}	$0.75^{+0.65}_{-0.56}$	12
J1112-6103	$5.26^{+5.15}_{-3.31} \times 10^{34}$	–	0.55 ± 0.54	0.55 ± 0.18	$9.85^{+9.83}_{-6.11} \times 10^{31}$	$1.09^{+0.65}_{-0.51}$	–	–	1
J1124-5916	$1.68^{+0.73}_{-0.6} \times 10^{35}$	1.5 ± 0.22	0.36 ± 0.09	0.41 ± 0.04	$1.13^{+0.65}_{-0.46} \times 10^{33}$	$0.94^{+0.07}_{-0.08}$	460^{+70}_{-80}	$0.34^{+0.34}_{-0.22}$	1
J1357-6429	$3.34^{+3.21}_{-2.11} \times 10^{34}$	–	0.35 ± 0.12	0.7 ± 0.12	$6.2^{+7.25}_{-3.94} \times 10^{31}$	$1.72^{+0.55}_{-0.63}$	140^{+60}_{-40}	$2.52^{+18.69}_{-2.54}$	13
J1418-6058	$9.20^{+9.72}_{-6.28} \times 10^{34}$	1.3 ± 0.2	1 ± 0.13	0.76 ± 0.05	$3.98^{+4.39}_{-2.65} \times 10^{31}$	$1.5^{+0.4}_{-0.4}$	–	–	14
J1420-6048	$4.94^{+4.74}_{-3.12} \times 10^{35}$	–	0.73 ± 0.18	0.78 ± 0.1	$3.75^{+3.6}_{-2.39} \times 10^{32}$	$0.63^{+0.33}_{-0.34}$	–	–	1
J1459-6053	$7.41^{+7.95}_{-5.06} \times 10^{34}$	1.6 ± 0.16	0.37 ± 0.07	0.44 ± 0.03	$4.38^{+4.72}_{-2.98} \times 10^{31}$	$1.08^{+0.18}_{-0.17}$	–	–	15
J1509-5850	$1.63^{+1.55}_{-1.05} \times 10^{35}$	1.5 ± 0.18	1.22 ± 0.13	0.53 ± 0.04	$7.13^{+6.86}_{-4.56} \times 10^{31}$	$1.9^{+0.12}_{-0.12}$	–	–	16
J1709-4429	$1.13^{+5.24}_{-4.25} \times 10^{36}$	1.3 ± 0.04	1.43 ± 0.02	0.37 ± 0.01	$1.82^{+0.86}_{-0.68} \times 10^{32}$	$1.62^{+0.2}_{-0.2}$	172^{+15}_{-14}	$2.08^{+2.92}_{-1.66}$	17
J1718-3825	$1.46^{+1.4}_{-0.93} \times 10^{35}$	1.3 ± 0.4	0.56 ± 0.14	0.68 ± 0.07	$6.48^{+6.26}_{-4.09} \times 10^{31}$	$1.62^{+0.33}_{-0.3}$	–	–	1
J1732-3131	$8.86^{+8.43}_{-5.64} \times 10^{33}$	0.37 ± 0.31	2.09 ± 0.05	1.04 ± 0.05	$3.07^{+3.01}_{-1.94} \times 10^{30}$	$1.14^{+0.35}_{-0.22}$	–	–	1
J1740+1000	$6.46^{+6.52}_{-4.04} \times 10^{32}$	–	0.33 ± 0.14	1.72 ± 0.98	$4.92^{+4.94}_{-3.04} \times 10^{30}$	$1.80^{+0.17}_{-0.17}$	83^{+5}_{-5}	$4.84^{+4.5}_{-3.65}$	18
J1741-2054	$1.29^{+5.39}_{-1.6} \times 10^{33}$	0.96 ± 0.15	0.84 ± 0.02	1.4 ± 0.05	$4.16^{+4}_{-2.74} \times 10^{30}$	$2.66^{+0.06}_{-0.06}$	60^{+2}_{-2}	$5.1^{+12.57}_{-3.7}$	19
J1747-2958	$1.22^{+1.16}_{-0.77} \times 10^{35}$	0.62 ± 0.54	0.53 ± 0.12	0.68 ± 0.06	$1.48^{+1.42}_{-0.96} \times 10^{33}$	$1.55^{+0.04}_{-0.04}$	–	–	20
J1801-2451	$5.50^{+5.38}_{-3.51} \times 10^{34}$	–	0.7 ± 0.47	0.46 ± 0.12	$1.53^{+1.47}_{-0.98} \times 10^{33}$	$1.6^{+0.6}_{-0.5}$	–	–	21

Table 2 – continued

Pulsars	L_γ (erg/sec)	Γ_{100}	E_p (GeV)	d_p	L_p (erg/sec)	Γ_p	kT (eV)	R (km)	References
J1809-2332	$1.45^{+2.18}_{-1.19} \times 10^{35}$	1.1 ± 0.12	1.29 ± 0.05	0.5 ± 0.02	$5.3^{+8.01}_{-4.28} \times 10^{31}$	$1.36^{+0.16}_{-0.15}$	178^{+23}_{-20}	$0.83^{+1.28}_{-0.79}$	1
J1813-1246	$2.08^{+0.22}_{-0.21} \times 10^{35}$	1.5 ± 0.12	0.48 ± 0.05	0.45 ± 0.02	$6.77^{+0.71}_{-0.68} \times 10^{32}$	$0.85^{+0.03}_{-0.03}$	–	–	1
J1826-1256	$6.01^{+0.4}_{-0.38} \times 10^{35}$	1.6 ± 0.1	0.87 ± 0.07	0.63 ± 0.03	$1.18^{+0.17}_{-0.16} \times 10^{32}$	$0.92^{+0.25}_{-0.24}$	–	–	22
J1833-1034	$1.8^{+0.3}_{-0.27} \times 10^{35}$	1.1 ± 0.76	0.31 ± 0.34	0.49 ± 0.15	$3.77^{+0.94}_{-0.82} \times 10^{33}$	$1.5^{+0.33}_{-0.31}$	–	–	1
J1836+5925	$1.85^{+2.9}_{-1.52} \times 10^{34}$	1.1 ± 0.03	1.48 ± 0.01	0.58 ± 0.01	$8.79^{+1.41}_{-6.86} \times 10^{29}$	$2.1^{+0.3}_{-0.3}$	45^{+10}_{-8}	$3.93^{+5.04}_{-1.71}$	23
J1838-0537	$2.32^{+2.55}_{-1.6} \times 10^{35}$	0.92 ± 0.66	1.28 ± 0.35	0.66 ± 0.09	$1.07^{+1.92}_{-0.79} \times 10^{32}$	1.2^{+1}_{-1}	–	–	24
J1907+0602	$2.42^{+2.32}_{-1.54} \times 10^{35}$	1.2 ± 0.16	0.95 ± 0.06	0.48 ± 0.02	$5.69^{+6}_{-3.52} \times 10^{31}$	$0.76^{+1.07}_{-0.34}$	–	–	1
J1952+3252	$1.62^{+2.83}_{-1.38} \times 10^{35}$	1.3 ± 0.12	0.99 ± 0.05	0.42 ± 0.02	$2.91^{+5.12}_{-2.47} \times 10^{33}$	$1.63^{+0.05}_{-0.05}$	130^{+20}_{-20}	$3.3^{+4.26}_{-2.04}$	25
J1957+5033	$9.44^{+21.3}_{-8.63} \times 10^{32}$	0.5 ± 0.4	0.76 ± 0.03	1.03 ± 0.07	$1.05^{+2.4}_{-0.94} \times 10^{30}$	$1.76^{+0.11}_{-0.11}$	54^{+5}_{-7}	$2.22^{+8.21}_{-1.91}$	26
J2021+3651	$1.9^{+4.59}_{-1.78} \times 10^{35}$	0.99 ± 0.1	1.06 ± 0.03	0.5 ± 0.01	$1.86^{+4.49}_{-1.72} \times 10^{31}$	$1.73^{+1.15}_{-1.02}$	159^{+17}_{-21}	$1.25^{+1.99}_{-0.68}$	27
J2021 + 4026 _{LGF}	$3.79^{+1.74}_{-1.43} \times 10^{35}$	1.662 ± 0.011	0.827 ± 0.002	–	$1.23^{+0.85}_{-0.58} \times 10^{31}$	$1^{+0.7}_{-0.8}$	210^{+30}_{-30}	$0.272^{+0.591}_{-0.255}$	28,29
J2021 + 4026 _{HGF}	$4.6^{+2.13}_{-1.72} \times 10^{35}$	1.639 ± 0.015	0.927 ± 0.003	–	$1.77^{+1.07}_{-0.76} \times 10^{31}$	$1.3^{+0.9}_{-0.9}$	210^{+40}_{-40}	$0.255^{+0.622}_{-0.245}$	30,31
J2022+3842	$3.24^{+2.33}_{-1.62} \times 10^{35}$	–	0.2 ± 0.22	0.61 ± 0.15	$7.69^{+5.45}_{-3.91} \times 10^{33}$	$1.23^{+0.22}_{-0.22}$	222^{+76}_{-37}	$5.23^{+16.5}_{-4.56}$	1
J2043+2740	$2.36^{+2.27}_{-1.52} \times 10^{33}$	–	0.83 ± 0.1	1.06 ± 0.18	$2.85^{+3.4}_{-1.82} \times 10^{30}$	$3.1^{+1.1}_{-0.6}$	–	–	32
J2055+2539	$2.28^{+1.29}_{-0.99} \times 10^{33}$	0.69 ± 0.17	1.21 ± 0.03	0.89 ± 0.04	$1.08^{+0.62}_{-0.47} \times 10^{30}$	$2.36^{+0.14}_{-0.14}$	–	–	33
J2229+6114	$2.58^{+2.48}_{-1.64} \times 10^{35}$	1.5 ± 0.07	0.74 ± 0.05	0.29 ± 0.01	$8.29^{+7.92}_{-5.28} \times 10^{32}$	$1.39^{+0.11}_{-0.12}$	126^{+19}_{-13}	$5.17^{+10.13}_{-3.99}$	1

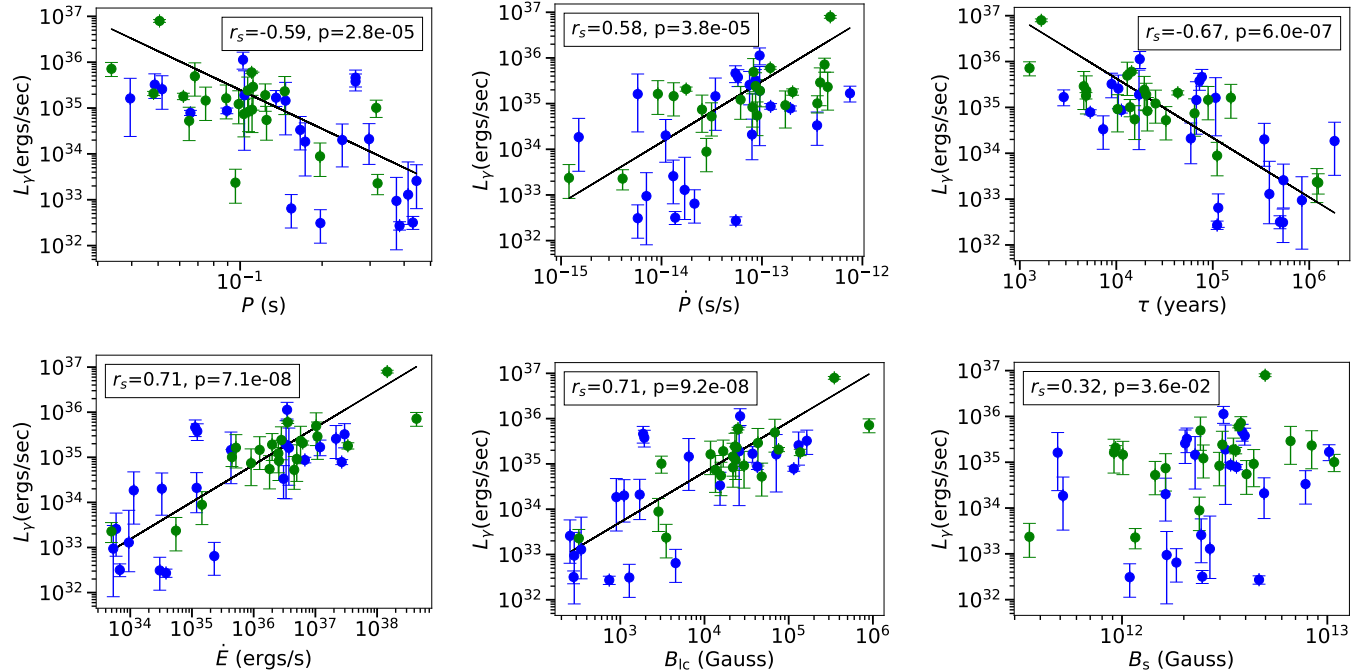


Figure 1. Gamma-ray luminosity (L_γ) versus timing parameters (P , \dot{P} , τ , \dot{E} , B_{lc} , B_s). r_s in the legend is the Spearman rank-order correlation coefficient, followed by its corresponding p-value. Green solid data points are for Group-1 pulsars (without detected thermal X-rays) and blue solid ones are for Group 2 (with detected thermal X-rays). These two groups do not distinguish themselves in these distributions. The straight line is the best linear fit.

in the X-ray spectrum, we found that the gamma-ray luminosity and the non-thermal X-ray luminosity are strongly correlated as shown in Fig. 2. A relationship between X-ray and gamma-ray luminosities has been reported as $L_{\text{X-ray}} \propto L_{\gamma}^{1.22 \pm 0.21}$ (Malov & Timirkeeva 2019). This relationship was obtained with the least-square method which only takes into account the error in the ordinate (y-direction). It gives an inconsistent relation when one interchanges the two luminosities from the ordinate to abscissa and vice versa. We use the orthogonal distance regression method which takes into account errors in both x- and y-directions to find the relationship from our sample. The best-fit relationship is given as

$$L_p \propto L_{\gamma}^{2.03 \pm 0.19} \quad (\chi_{\nu}^2 = 23.1) . \quad (7)$$

The best fit for its inverse relationship, that is, putting L_{γ} in the ordinate and L_p in the abscissa, is given as

$$L_{\gamma} \propto L_p^{0.49 \pm 0.05} \quad (\chi_{\nu}^2 = 23.1) , \quad (8)$$

which is consistent with Eq.(7).

As one can see from Fig. 2, pulsars without and with detected thermal emission seem to show different dependence between L_{γ} and L_p . We designate these two groups of pulsars as Group 1 (without detected thermal emission) and Group 2 (with detected thermal emission). The best-fit relationships between L_{γ} and L_p for these two groups are

$$L_{\gamma} \propto L_p^{0.34 \pm 0.04} \quad (\chi_{\nu}^2 = 17.4) \quad (\text{Group 1}), \quad (9)$$

and

$$L_{\gamma} \propto L_p^{0.86 \pm 0.14} \quad (\chi_{\nu}^2 = 9.8) \quad (\text{Group 2}). \quad (10)$$

It is important to note that while the non-thermal X-ray luminosity is correlated with the gamma-ray luminosity, the gamma-ray energy flux shows no correlation with radio flux density, as shown in Fig. 6 of the 3PC.

For the rest of the gamma-ray spectral parameters (E_p , Γ_{100} and d_p), the two groups separately do not show a strong correlation, except for E_p versus L_p in Group 1 pulsars (the lower left panel in Fig. 2) The relationship for these gamma-ray spectral parameters with L_p is given below for readers' reference:

$$\Gamma_{100} = (0.2 \pm 0.03) \log L_p + (-5.04 \pm 1.03) \quad (\chi_{\nu}^2 = 8.2) , \quad (11)$$

$$E_p \propto L_p^{-0.40 \pm 0.12} \quad (\chi_{\nu}^2 = 15.4) , \quad (12)$$

and

$$d_p \propto L_p^{-0.12 \pm 0.02} \quad (\chi_{\nu}^2 = 10.4) . \quad (13)$$

The correlation of gamma-ray spectral parameters with non-thermal X-ray photon index (Γ_p) is shown in Fig. 3, in which one can see that only gamma-ray luminosity has an strong anti-correlation with the X-ray photon index with a Spearman coefficient of -0.64, whose best fit to describe the correlation is

$$\log L_{\gamma} = (-1.94 \pm 0.28) \Gamma_p + (37.53 \pm 0.35) \quad (\chi_{\nu}^2 = 5.2) . \quad (14)$$

It means that the luminosity of gamma rays increases when the non-thermal X-rays becomes harder. A similar anti-correlation between L_p and Γ_p was reported in Chang et al. (2023). Given the positive correlation between L_{γ} and L_p , it is not surprising to see the anti-correlation between L_{γ} and Γ_p . However, what these relations imply is yet to be revealed. It is also interesting to check whether this relation differs between Group-1 and -2 pulsars. If fitted separately, the best fits are

$$\log L_{\gamma} = (-2.03 \pm 0.49) \Gamma_p + (37.5 \pm 0.5) \quad (\chi_{\nu}^2 = 7.5) \quad (\text{Group 1}),$$

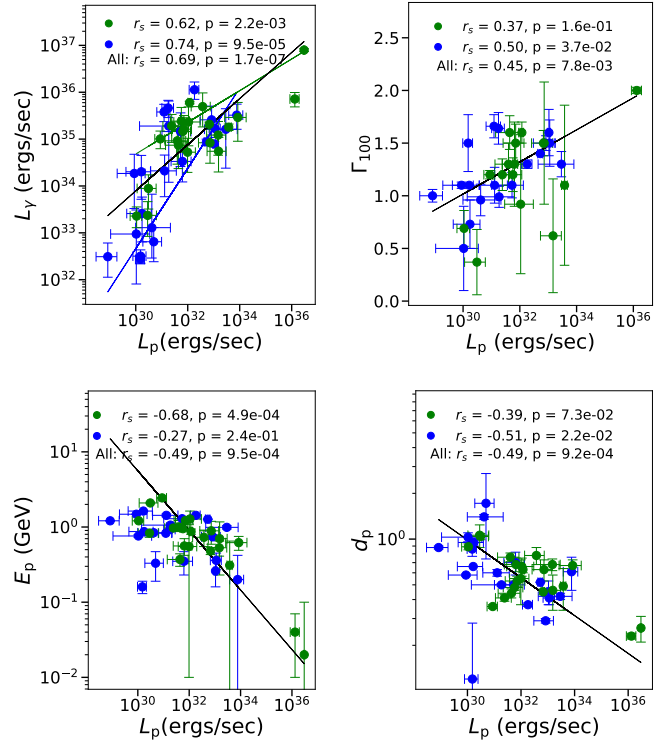


Figure 2. Gamma-ray spectral parameters versus non-thermal X-ray luminosity (L_p). r_s in the legend is the Spearman rank-order correlation coefficient, followed by its corresponding p-value. Green solid data points are for Group-1 pulsars (without detected thermal X-rays) and blue solid ones are for Group-2 (with detected thermal X-rays). The black line indicates the best-fit for all data points, green line indicates the best-fit for Group 1 data and blue line indicates the best-fit for Group 2 data.

$$(15)$$

and

$$\log L_{\gamma} = (-2.65 \pm 0.57) \Gamma_p + (38.72 \pm 0.85) \quad (\chi_{\nu}^2 = 2.6) \quad (\text{Group 2}), \quad (16)$$

which do not show a statistically significant difference.

To explore the dependence of L_{γ} on L_p and Γ_p jointly, we adopt a function form like the following and their best fits are given as

$$L_{\gamma} \propto L_p^{(0.33 \pm 0.04)} e^{(-1.03 \pm 0.15) \Gamma_p} \quad (\chi_{\nu}^2 = 2.9) , \quad (17)$$

$$L_{\gamma} \propto L_p^{(0.34 \pm 0.04)} e^{(-0.84 \pm 0.18) \Gamma_p} \quad (\chi_{\nu}^2 = 2.6) \quad (\text{Group 1}) \quad (18)$$

and

$$L_{\gamma} \propto L_p^{(0.21 \pm 0.14)} e^{(-1.83 \pm 0.48) \Gamma_p} \quad (\chi_{\nu}^2 = 2.6) \quad (\text{Group 2}). \quad (19)$$

In all the above relationships, that is, $L_{\gamma}(L_p)$, $L_{\gamma}(\Gamma_p)$ and $L_{\gamma}(L_p, \Gamma_p)$, Group-2 pulsars seem to have a more sensitive dependence than Group 1, although it is only more apparent to separate these two group in $L_{\gamma}(L_p)$. Other gamma-ray spectral parameters as a function of L_p and Γ_p jointly are listed below:

$$\Gamma_{100} \propto L_p^{(0.15 \pm 0.01)} e^{(-0.27 \pm 0.08) \Gamma_p} \quad (\chi_{\nu}^2 = 1.6) , \quad (20)$$

$$\Gamma_{100} \propto L_p^{(0.17 \pm 0.02)} e^{(-0.26 \pm 0.12) \Gamma_p} \quad (\chi_{\nu}^2 = 1.4) \quad (\text{Group 1}) \quad (21)$$

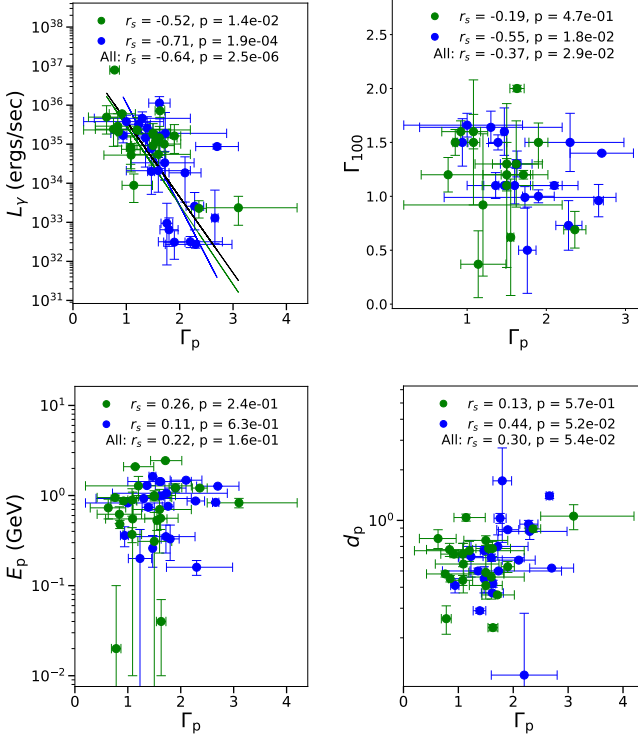


Figure 3. Gamma-ray spectral parameters vs non-thermal X-ray photon index (Γ_p). Legends are the same as previous figures.

and

$$L_{100} \propto L_p^{(0.12 \pm 0.03)} e^{(-0.32 \pm 0.15)\Gamma_p} \quad (\chi^2_\nu = 1.8) \quad (\text{Group 2}) . \quad (22)$$

$$E_p \propto L_p^{(-0.42 \pm 0.1)} e^{(-0.63 \pm 0.19)\Gamma_p} \quad (\chi^2_\nu = 4.3) , \quad (23)$$

$$E_p \propto L_p^{(-0.37 \pm 0.07)} e^{(-0.35 \pm 0.13)\Gamma_p} \quad (\chi^2_\nu = 2.3) \quad (\text{Group 1}) \quad (24)$$

and

$$E_p \propto L_p^{(-0.26 \pm 0.13)} e^{(0.47 \pm 0.26)\Gamma_p} \quad (\chi^2_\nu = 13.2) \quad (\text{Group 2}) . \quad (25)$$

$$d_p \propto L_p^{(-0.07 \pm 0.01)} e^{(0.24 \pm 0.05)\Gamma_p} \quad (\chi^2_\nu = 6.1) , \quad (26)$$

$$d_p \propto L_p^{(-0.11 \pm 0.02)} e^{(-0.17 \pm 0.06)\Gamma_p} \quad (\chi^2_\nu = 7.1) \quad (\text{Group 1}) \quad (27)$$

and

$$d_p \propto L_p^{(-0.12 \pm 0.02)} e^{(0.15 \pm 0.07)\Gamma_p} \quad (\chi^2_\nu = 3.9) \quad (\text{Group 2}) . \quad (28)$$

3.3 Correlation between gamma-ray spectral parameters and thermal X-ray spectral parameters

Among our samples, 22 pulsars exhibit thermal emission. The correlations between the gamma-ray spectral parameters (L_γ , Γ_{100} , d_p , E_p) and the thermal X-ray spectral parameters (kT , R) are shown in Figs. 4 and 5.

As discussed earlier, we expect to see a relation between gamma-ray luminosity and thermal emission properties (kT , R), since thermal photons from the stellar surface may play a certain role in pair

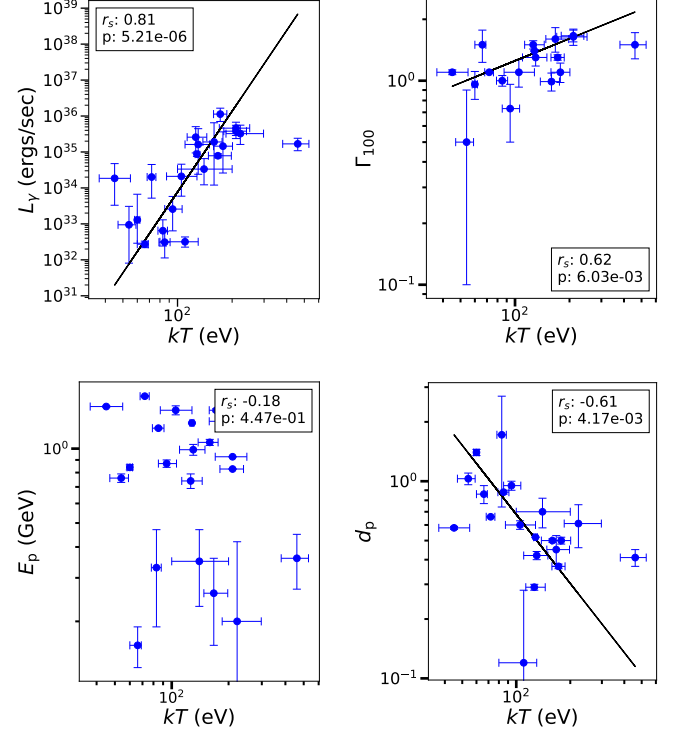


Figure 4. Gamma-ray spectral parameters versus blackbody temperature (kT)

production in pulsars', such as providing photons for two-photon pair production in the outer-gap model and cooling the pairs created in the polar gap region with inverse Compton scattering (e.g. Cheng et al. (1986); Chang (1995)). Thermal emissions of 22 pulsars in this sample are detected and their correlation with the gamma-ray luminosity is shown in Fig. 4 & 5, where one can see that the gamma-ray spectral properties are not correlated with the radius of the emitting region R but there is a strong correlation between the gamma-ray luminosity and the temperature of the thermal emission, indicated by a Spearman coefficient of 0.81 (p-value of about 10^{-6}). E_p shows no correlation, while d_p and Γ_{100} shows a correlation with weak significance and their best fit is described by

$$L_\gamma \propto kT^{7.24 \pm 1.17} \quad (\chi^2_\nu = 4.8) . \quad (29)$$

$$\Gamma_{100} = (1.12 \pm 0.21) \log kT + (-0.98 \pm 0.42) \quad (\chi^2_\nu = 4.7) \quad (30)$$

$$d_p \propto kT^{-1.2 \pm 0.2} \quad (\chi^2_\nu = 8.3) \quad (31)$$

We further examine the relation between the gamma-ray spectral parameters and both thermal parameters, kT and R , jointly in a 3-dimensional space, since gamma-ray emissions very likely depend not only on the surface temperature but also on the flux level of thermal photons. The best fit to describe their relationship is found to be the following:

$$L_\gamma \propto kT^{4.79 \pm 0.90} R^{2.55 \pm 0.58} \quad (\chi^2_\nu = 0.54) . \quad (32)$$

This fitting has a χ^2_ν of 0.54, showing improvement over Eq.(29) by adding one more parameter (R). The significance of this improvement can be checked with the F-test, which indicates a very significant improvement at a random probability much lower than 10^{-5} . It suggests a fundamental plane in the space of $\{L_\gamma, kT, R\}$, as shown in Fig.

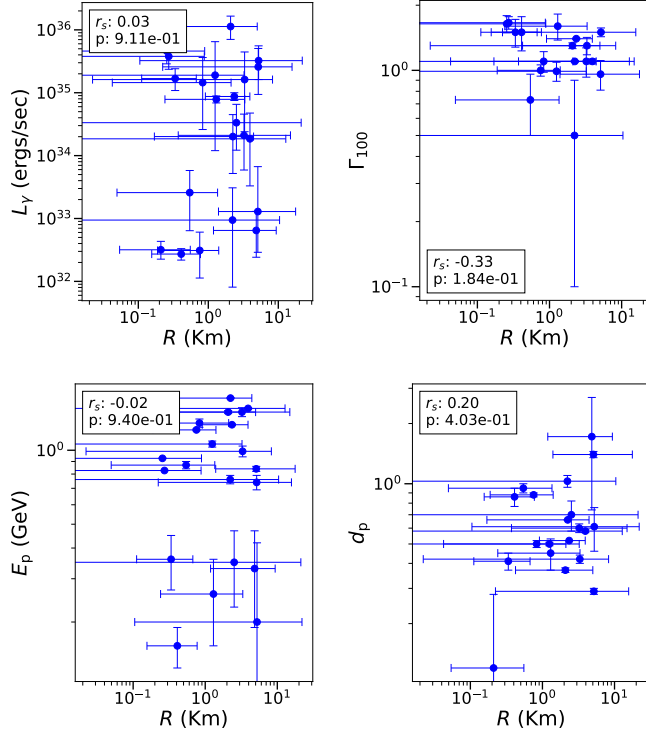


Figure 5. Gamma-ray spectral parameters versus blackbody radius (R)

6. We note, however, the statistical statement here is only suggestive, as discussed earlier.

In fact, we also found that the nonthermal X-ray luminosity of these Group-2 pulsars follows a relationship of $L_p \propto kT^{5.97 \pm 1.08} R^{3.28 \pm 0.77}$ ($\chi^2 = 0.42$). This relationship is consistent with Eq.(11) in Chang et al. (2023). The sample used in this study is a subset of that used in Chang et al. (2023). It is also compatible with Eqs.(32) and (10).

Since the gamma-ray spectral parameters (E_p , d_p , Γ_{100}) do not exhibit a strong correlation with surface temperature, we further investigate their relationships with the two thermal parameters jointly. The resulting correlation is illustrated in Fig. 6. Their corresponding best-fit descriptions are shown in the following.

$$\Gamma_{100} = \log((kT)^{1.96 \pm 0.64} R^{0.39 \pm 0.30}) + (-2.89 \pm 1.36) \quad (\chi^2 = 0.67) \quad (33)$$

$$E_p \propto kT^{1.28 \pm 1.12} R^{2.26 \pm 1.34} \quad (\chi^2 = 0.64) \quad (34)$$

$$d_p \propto kT^{-0.56 \pm 0.16} R^{-0.37 \pm 0.11} \quad (\chi^2 = 0.76) \quad (35)$$

As shown by the above equations, the gamma-ray spectral parameters (L_γ , Γ_{100} , E_p , d_p) exhibit improved fits, indicated by lower reduced chi-square values, when the blackbody radius (R) is included in addition to the blackbody temperature (kT).

3.4 Correlations among gamma-ray spectral parameters

The correlations among the gamma-ray spectral parameters are shown in Fig. 7. Except for L_γ versus d_p and Γ_{100} versus d_p , no clear correlations are found among them. There is no indication for

Group 1 and Group 2 pulsars having different behavior either. The best fit relationships for those having a more significant correlation are listed below:

$$L_\gamma \propto d_p^{-5.98 \pm 0.8} \quad (\chi^2 = 6.68) \quad (36)$$

$$\log L_\gamma = (2.35 \pm 0.36) \Gamma_{100} + (31.74 \pm 0.53) \quad (\chi^2 = 3.61) \quad (37)$$

$$\Gamma_{100} = (-1.72 \pm 0.22) \log d_p + (0.83 \pm 0.06) \quad (\chi^2 = 9.66) \quad (38)$$

4 DISCUSSION

Because of unknown beaming factors, viewing geometry and distance uncertainties, there is usually a large scatter in the correlation among spectral and timing properties (Possenti et al. 2002; Li et al. 2008; Kalapotharakos et al. 2022; Chang et al. 2023). All the statistical descriptions of correlation function forms obtained from best fits are therefore only suggestive. These correlations are, however, still helpful in illustrating possible trends and dependencies among spectral and timing properties. It may inspire or constrain theoretical models of pulsar emissions.

In the sample we studied, clear correlations are found for the gamma-ray luminosity with pulsars' age, spindown power and magnetic field strength at the light cylinder. It is worth noting that it does not correlate with the magnetic field strength at the stellar surface (see Fig. 1), similar to the non-thermal X-ray luminosity (Chang et al. 2023). Although actual physical mechanisms need to be modeled, it seems that both the gamma-ray and non-thermal X-ray luminosities are more linked to outer magnetospheres or the wind zones of pulsars. Other gamma-ray spectral parameters, Γ_{100} , E_p and d_p , do not show such a clear correlation.

The main purpose of this paper is to investigate possible correlations between the gamma-ray and X-ray spectral properties. We found that L_γ has a strong correlation with the non-thermal X-ray luminosity L_p and it goes like $L_\gamma \propto L_p^{0.49 \pm 0.05}$, or tentatively, $L_\gamma \propto L_p^{0.5}$. While the non-thermal X-ray luminosity and gamma-ray luminosity are correlated, the gamma-ray energy flux shows no correlation with the radio flux density, as reported in the 3PC. This is one of the major results obtained in this study. Non-thermal X-rays from pulsars are usually attributed to synchrotron radiation of electron-positron pairs right after they are created somewhere in the magnetosphere of pulsars or to the low-energy continuum tail of a broad-band high-energy emission, which peaks around GeV. The X-ray power-law component of some pulsars obviously represent a separate component from the gamma-ray one in the broadband SED, but some others seem to have the non-thermal X-ray and gamma-ray emissions forming a single component in pulsar broadband spectra. The broadband spectra for the listed pulsars are shown in Figs. 8 and 9. The X-ray spectra in the 0.5–10 keV range are plotted using the spectral indices provided in Table 2. Fig. 8 is for Group-1 pulsars and Fig. 9 is for Group 2. For energies above 100 MeV, the spectra are taken from the Fermi 3PC catalog, and for the intermediate energy range (0.01–100 MeV), the spectra are based on face values taken from figures in Coti Zelati et al. (2020). Although spectral fitting uncertainties hinder a clear conclusion, one can see from Figs. 8 and 9 that X-ray emissions of some pulsars, such as J0007+7303, J2043+2740, J1509–5850, J1718–3825, J0357+3205, and J2021+3651, do not form a single spectral component with their gamma-ray emissions. More observations in the soft

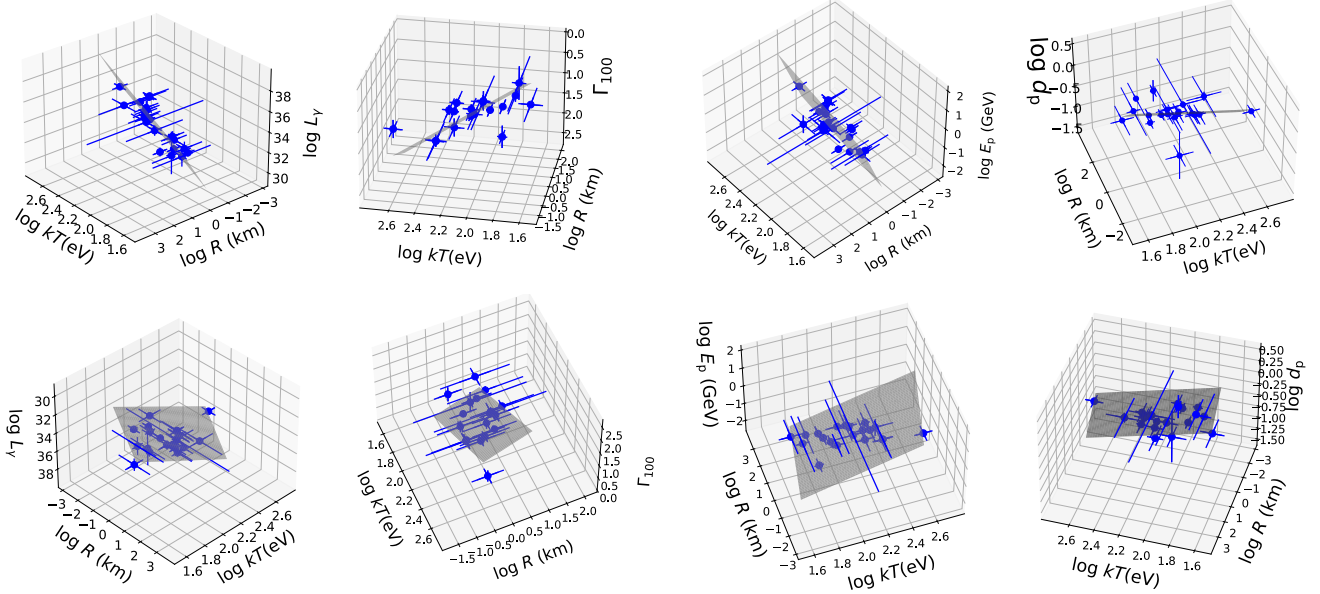


Figure 6. Fundamental planes of gamma-ray spectral parameters (L_γ , Γ_{100} , E_p , d_p) in the space of thermal parameters (kT , R). The first row shows the edge-on view of the plane and the second row shows the top-on view of the plane.

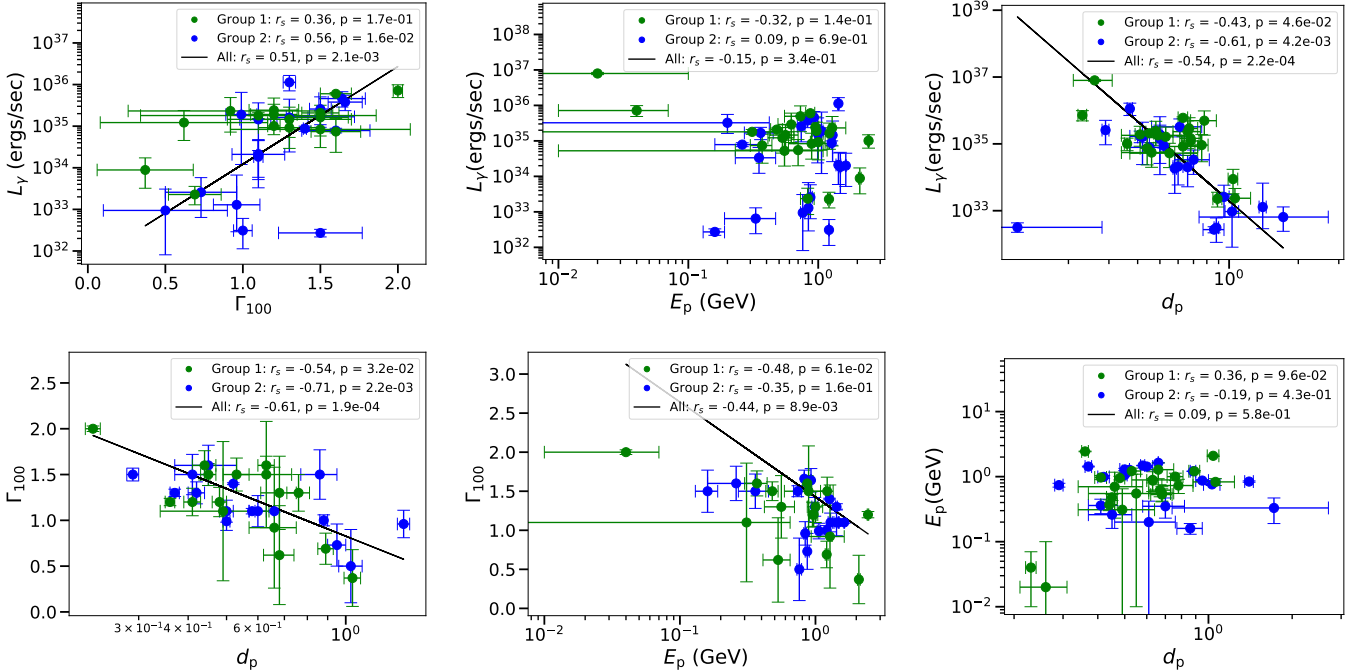


Figure 7. Correlations between Gamma-ray spectral parameters

gamma-ray regime will help identify if the other pulsars have a single spectral component from X-ray to gamma rays. In any case, however, the relation that $L_\gamma \propto L_p^{0.5}$ seems to indicate that the non-thermal X-ray emission is not simply the low-energy tail of the gamma-ray emission. They could be related to each other in a more complicated way through radiating-particle initial energy distribution (right after their creation), acceleration mechanisms after/during synchrotron cooling and the gamma-ray radiation mechanisms.

An interesting result is that pulsars without (Group 1) and with

(Group 2) detected thermal emissions seem to distinguish themselves in their relationships of L_γ versus L_p ; see Fig. 2, Eq. 9 and 10. If it is indeed the case, which requires a larger sample to verify, it strongly suggests that pulsars of Groups 1 and 2 are from different populations. It is clear that gamma-ray emission is related to X-ray emission and the relation changes when thermal emission is present. This confirms that thermal X-rays do play a role in the emission of non-thermal X-rays and gamma rays, since its presence makes a difference. Another interesting issue is why the surface thermal emission of Group-1

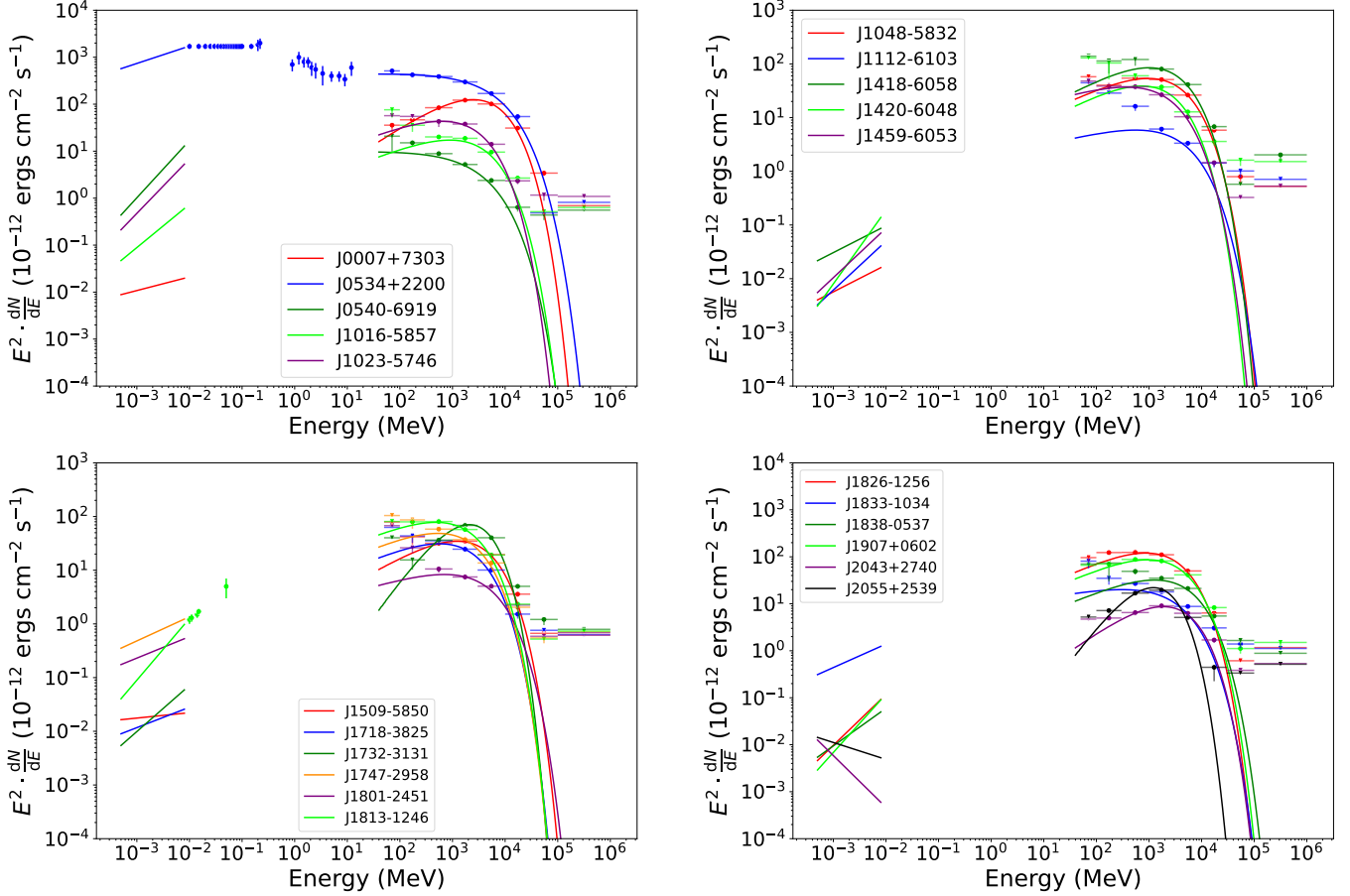


Figure 8. Broad-band spectra of Group-1 pulsars.

pulsars is not detected. These two groups do not show different distributions in timing parameters. There is no indication of data quality difference for these two groups either. The non-detection of a thermal component is not due to data quality. In particular, Group-1 pulsars are not older. There is no reason for those pulsars to have a lower surface temperature and smaller thermal luminosity so that detection is more difficult, unless they have a cooling curve different from that of Group-2 pulsars. It is tempting to investigate whether they are actually quark stars rather than neutron stars or they cool down through a more exotic process; see, e.g., [Slane et al. \(2002\)](#), [Potekhin et al. \(2020\)](#) and [Zapata et al. \(2022\)](#).

A strong anticorrelation is also found between L_γ and the photon index Γ_p of the power-law component in X-rays (Fig. 3). This is not surprising since a similar anti-correlation is also reported in [Chang et al. \(2023\)](#) between L_p and Γ_p and we have $L_\gamma \propto L_p^{0.5}$ here. A harder X-ray spectrum comes with a higher gamma-ray and non-thermal X-ray luminosities. This may have some implications on the physical conditions of their acceleration and emission mechanisms. A best-fit function form of $L_\gamma(L_p, \Gamma_p)$ is shown in Eq. 17. It may **provide some constraints** on future modeling works. The aforementioned Group 1 and Group 2 pulsars do not show statistically significant distinctions in these relations involving Γ_p .

The strong correlation between L_γ and the stellar surface temperature, represented by kT throughout this paper, is noteworthy. Similarly to L_p , studied in [Chang et al. \(2023\)](#) with a larger sample, L_γ shows a strong dependence on temperature kT but not on the emission-region radius R and a much better fit can be found when

the dependence on both kT and R is taken into account at the same time. This indicates a possible connection between thermal photons and high-energy emissions. As discussed in [Chang et al. \(2023\)](#) and references therein, ideas of pair production near the polar cap region and in the outer-gap region have been investigated for a long time. In either locations thermal photons both play a role in pair production via inverse Compton scattering or two-photon pair production. A clear dependence function form may help to model these processes. Unfortunately, a precise and more statistically reliable description of the fundamental planes in the spaces of $\{L_\gamma, kT, R\}$ or $\{L_p, kT, R\}$ has yet to come with improved measurement uncertainties.

ACKNOWLEDGEMENTS

This work was supported by the National Science and Technology Council (NSTC) of the Republic of China (Taiwan) under grant NSTC 114-2112-M-007-042.

DATA AVAILABILITY

The data employed by this article are available in the article and in the quoted references.

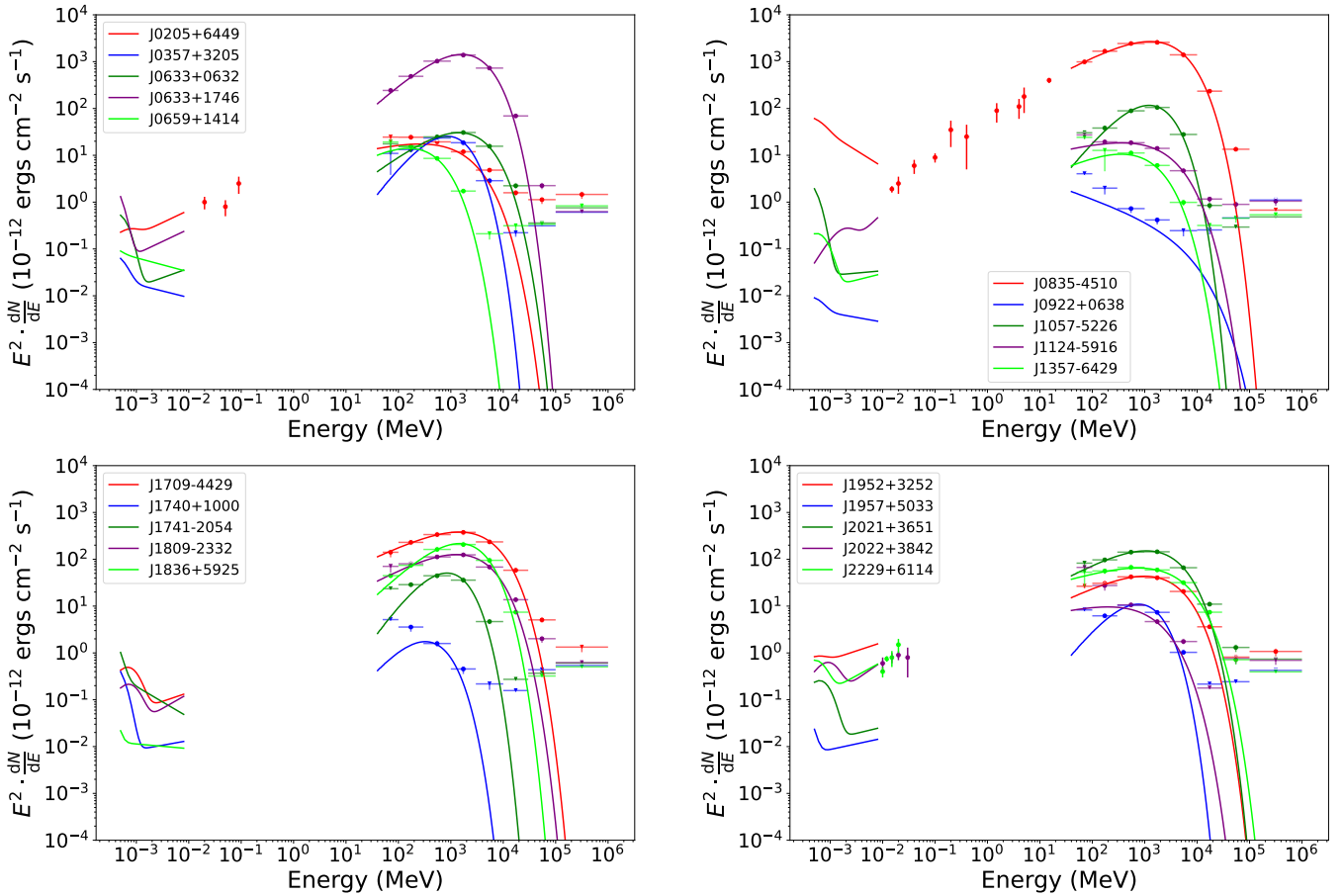


Figure 9. Broad-band spectra of Group-2 pulsars.

REFERENCES

Abdo A. A., et al., 2013, *ApJS*, **208**, 17

Allafort A., et al., 2013, *ApJ*, **777**, L2

Arons J., 1983, *ApJ*, **266**, 215

Barnard M., Venter C., Harding A. K., Kalapotharakos C., Johnson T. J., 2022, *ApJ*, **925**, 184

Becker W., Weisskopf M. C., Tennant A. F., Jessner A., Dyks J., Harding A. K., Zhang S. N., 2004, *ApJ*, **615**, 908

Cerutti B., Figueiredo E., Dubus G., 2025, *A&A*, **695**, A93

Chang H.-K., 1995, *A&A*, **301**, 456

Chang C., Pavlov G. G., Kargaltsev O., Shibanov Y. A., 2012, *ApJ*, **744**, 81

Chang H.-K., Hsiang J.-Y., Chu C.-Y., Chung Y.-H., Su T.-H., Lin T.-H., Huang C.-Y., 2023, *MNRAS*, **520**, 4068

Cheng K. S., Ho C., Ruderman M., 1986, *ApJ*, **300**, 500

Coroniti F. V., 1990, *ApJ*, **349**, 538

Coti Zelati F., Torres D. F., Li J., Viganò D., 2020, *MNRAS*, **492**, 1025

Danilenko A., Shternin P., Karpova A., Zyuzin D., Shibanov Y., 2015, *Publ. Astron. Soc. Australiæ*, **32**, e038

Daugherty J. K., Harding A. K., 1982, *ApJ*, **252**, 337

De Luca A., Caraveo P. A., Mereghetti S., Negroni M., Bignami G. F., 2005, *ApJ*, **623**, 1051

Ge M. Y., et al., 2019, *Nature Astronomy*, **3**, 1122

Harding A. K., Venter C., Kalapotharakos C., 2021, *ApJ*, **923**, 194

Íñiguez-Pascual D., Viganò D., Torres D. F., 2022, *MNRAS*, **516**, 2475

Kalapotharakos C., Wadiasingh Z., Harding A. K., Kazanas D., 2022, *ApJ*, **934**, 65

Kargaltsev O., Pavlov G. G., Garmire G. P., 2007, *ApJ*, **660**, 1413

Karpova A., Danilenko A., Shibanov Y., Shternin P., Zyuzin D., 2014, *ApJ*, **789**, 97

Karpova A. V., Zyuzin D. A., Shibanov Y. A., 2019, *MNRAS*, **487**, 1964

Kaspi V. M., Gotthelf E. V., Gaensler B. M., Lyutikov M., 2001, *ApJ*, **562**, L163

Kim M., An H., 2020, *ApJ*, **892**, 5

Kirk J. G., Skjæraasen O., Gallant Y. A., 2002, *A&A*, **388**, L29

Klingler N., et al., 2016, *ApJ*, **833**, 253

Klingler N., Kargaltsev O., Pavlov G. G., Ng C. Y., Beniamini P., Volkov I., 2018, *ApJ*, **861**, 5

Klingler N., Kargaltsev O., Pavlov G. G., Ng C. Y., Gong Z., Hare J., 2022, *ApJ*, **932**, 89

Li X. H., Lu F. J., Li T. P., 2005, *ApJ*, **628**, 931

Li X.-H., Lu F.-J., Li Z., 2008, *ApJ*, **682**, 1166

Lin L. C. C., et al., 2013, *ApJ*, **770**, L9

Lin L. C. C., Hui C. Y., Li K. T., Takata J., Hu C. P., Kong A. K. H., Yen D. C. C., Chou Y., 2014, *ApJ*, **793**, L8

Malov I. F., Timirkieva M. A., 2019, *MNRAS*, **485**, 5319

Manchester R. N., Hobbs G. B., Teoh A., Hobbs M., 2005, *AJ*, **129**, 1993

Marelli M., et al., 2013, *ApJ*, **765**, 36

Marelli M., Pizzocaro D., De Luca A., Gastaldello F., Caraveo P., Saz Parkinson P., 2016, *ApJ*, **819**, 40

Mayer M. G. F., Becker W., 2024, *A&A*, **684**, A208

Michel F. C., 1994, *ApJ*, **431**, 397

Pancreazi B., et al., 2012, *A&A*, **544**, A108

Pavlov G. G., Zavlin V. E., Sanwal D., Burwitz V., Garmire G. P., 2001, *ApJ*, **552**, L129

Pétri J., 2024, *A&A*, **687**, A169

Posselt B., Spence G., Pavlov G. G., 2015, *ApJ*, **811**, 96

Posselt B., et al., 2017, *ApJ*, **835**, 66

Possenti A., Cerutti R., Colpi M., Mereghetti S., 2002, *A&A*, **387**, 993

Potekhin A. Y., Zyuzin D. A., Yakovlev D. G., Beznogov M. V., Shibanov

Y. A., 2020, *MNRAS*, **496**, 5052
 Rigoselli M., Mereghetti S., 2018, *A&A*, **615**, A73
 Rigoselli M., Mereghetti S., Anzuinelli S., Keith M., Taverna R., Turolla R., Zane S., 2022, *MNRAS*, **513**, 3113
 Romani R. W., Ng C. Y., Dodson R., Brisken W., 2005, *ApJ*, **631**, 480
 Slane P. O., Helfand D. J., Murray S. S., 2002, *ApJ*, **571**, L45
 Smith D. A., et al., 2023, *ApJ*, **958**, 191
 Takata J., Cheng K. S., 2017, *ApJ*, **834**, 4
 Torres D. F., Viganò D., Coti Zelati F., Li J., 2019, *MNRAS*, **489**, 5494
 Van Etten A., Romani R. W., Ng C. Y., 2008, *ApJ*, **680**, 1417
 Wang H. H., Takata J., Hu C. P., Lin L. C. C., Zhao J., 2018, *ApJ*, **856**, 98
 Wang H. H., Takata J., Lin L. C. C., Tam P. H. T., 2024, *MNRAS*, **527**, 12016
 Watters K. P., Romani R. W., Weltevrede P., Johnston S., 2009, *ApJ*, **695**, 1289
 Xu Y.-J., Peng H.-L., Weng S.-S., Zhang X., Ge M.-Y., 2025, *ApJ*, **981**, 100
 Zapata J., Sales T., Jaikumar P., Negreiros R., 2022, *A&A*, **663**, A19
 Zhao J., et al., 2017, *ApJ*, **842**, 53
 Zyuzin D. A., Karpova A. V., Shibanov Y. A., Potekhin A. Y., Suleimanov V. F., 2021, *MNRAS*, **501**, 4998

APPENDIX A:

The relationships between gamma-ray spectral parameters Γ_{100} , E_p , d_p and timing parameters are in weak or negligible, unlike L_γ , as described in the main text. These are shown in this Appendix. Those relationships with a p-value $\leq 10^{-2}$ are given a best fit description in the following:

$$\Gamma_{100} = (0.095 \pm 0.037) \log \dot{E} + (-1.96 \pm 1.31) \quad (\chi^2_\nu = 61.9) \quad (\text{A1})$$

$$\Gamma_{100} = (0.11 \pm 0.05) \log B_{\text{lc}} + (1.00 \pm 0.20) \quad (\chi^2_\nu = 66.1) \quad (\text{A2})$$

$$E_p \propto P^{-0.38 \pm 0.13} \quad (\chi^2_\nu = 511.8) \quad (\text{A3})$$

$$E_p \propto \dot{E}^{-0.019 \pm 0.032} \quad (\chi^2_\nu = 613.0) \quad (\text{A4})$$

$$E_p \propto B_{\text{lc}}^{-0.022 \pm 0.049} \quad (\chi^2_\nu = 616.0) \quad (\text{A5})$$

$$d_p \propto P^{0.245 \pm 0.002} \quad (\chi^2_\nu = 51.1) \quad (\text{A6})$$

$$d_p \propto \dot{P}^{0.099 \pm 0.001} \quad (\chi^2_\nu = 61.5) \quad (\text{A7})$$

$$d_p \propto \dot{E}^{0.045 \pm 0.001} \quad (\chi^2_\nu = 50.7) \quad (\text{A8})$$

$$d_p \propto \tau^{0.070 \pm 0.001} \quad (\chi^2_\nu = 54.4) \quad (\text{A9})$$

$$d_p \propto B_{\text{lc}}^{-0.066 \pm 0.002} \quad (\chi^2_\nu = 50.0) \quad (\text{A10})$$

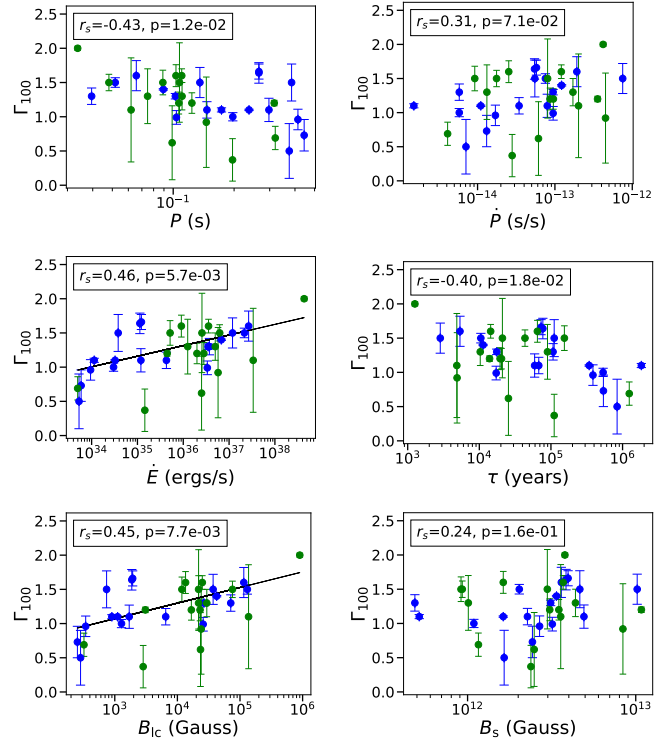


Figure A1. Γ_{100} vs timing parameters

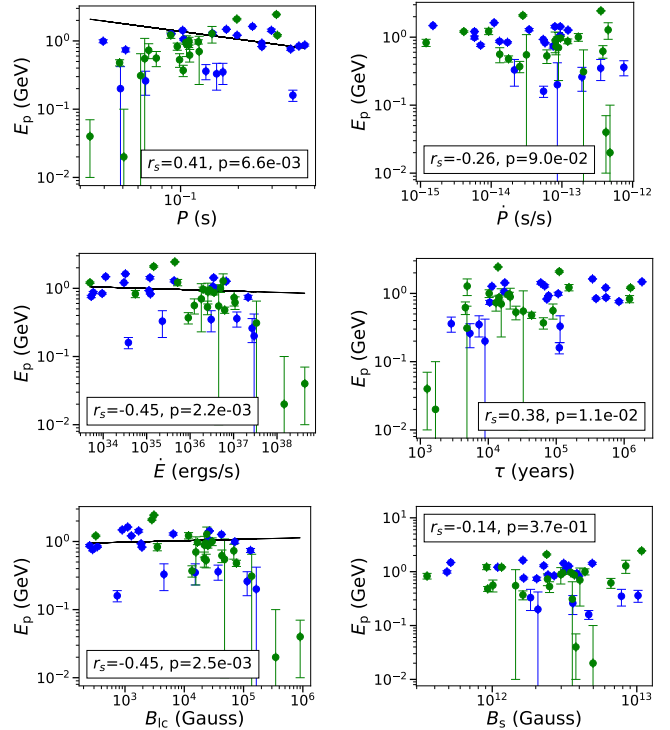


Figure A2. E_p vs timing parameters

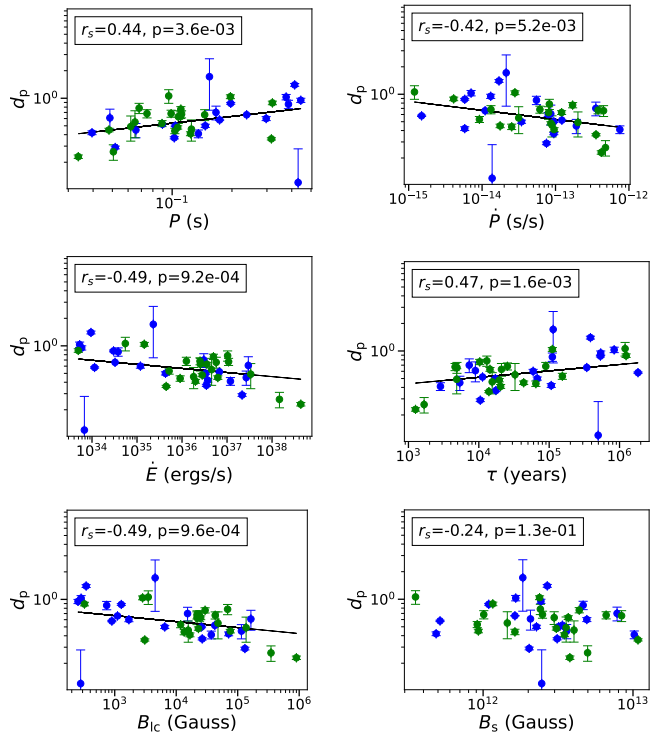


Figure A3. d_p vs timing parameters